1   **The Characterization of Chloride Effect on Concrete Water Sorption and its**

2   **Application in the Modelling of Concrete Conditions in Tidal Zones**

3

4   *Yu Wang[1], Hayder Oleiwi[2], Chung-Yue Wang[3], Nan Xiang[4], Jian Geng[5]

5

6   1. School of Science, Engineering & Environment, University of Salford, Manchester M5 4WT,

7   UK

8   2. College of Engineering, University of Thi-Qar, Nasiriyah, Iraq

9   3. Department of Civil Engineering, National Central University, Taiwan, R. China

10   4. School of Civil Engineering, Chongqing Jiao Tong University, Chongqing, PR. China

11   5. Centre of Green Building Materials and Waste Resources Reuse, Ningbo Institute of

12   Technology, Zhejiang University, PR. China

13

14   *Corresponding Author: y.wang@salford.ac.uk

15

16   **Abstract**

17   Concrete exposed to cyclic wetting and drying in salty water conditions is thought to be subjected

18   to an accelerated ingress of chloride from the outside environment, and prone to a worsening

19   deterioration process inside. Additionally, there is an osmotic effect on salty water flow in porous

20   concrete. However, so far, a fully profound understanding of the coupled cyclic wetting-drying

21   and osmosis effects on the chloride movement in concrete is still limited. This paper reports on a

22   comprehensive study on the topic. A series of experimental tests was conducted initially for the

23   vapour-water sorption isotherm (VWSI) of normal concrete of different porosity and chloride

24   content. Thereafter, a novel mathematical model was proposed and validated to characterise the

25   effect of chloride salt on the vapour absorption and water retention behaviour of concrete. Finally,

26   the proposed characteristic model was implemented in a numerical model to simulate chloride

27   ingress in concrete in tidal zones. The vapour-water sorption isotherm model successfully provides

28   an effective tool to quantify the coupled influence of cyclic wetting-drying and osmosis on chloride

29   transportation in concrete.

30

31   **Keywords**: Concrete, Chloride, Osmotic effect, Unsaturated suction, Water saturation.

32

1. Introduction

34 Chloride plays an important role in the rebar corrosion of reinforced concrete structures serving in

35 saline environments. The time taken for chloride from the outside environment to reach the surface

36 of reinforcement in concrete structures to a critical amount decisively influences the total life span

37 of these structures. Predicting and making an assessment on chloride transport in concrete has been

38 a topical research since the end of last century [1-5]. Since then it has been widely recognised that

39 chloride ingress in concrete from external saline environments is mainly driven by pore water

40 infiltration and chloride diffusion [6.7]. Meanwhile, there are many factors which have direct

41 influences on these two major mechanisms, such as temperature, carbonation and the local

42 electrochemical potential gradient [3,8,9]. In addition, it has been noted that structures exposed to

43 cyclic wetting and drying conditions are subject to accelerated chloride penetration under the

44 entangled effects of diffusion and convection mechanisms [10-12].

45 Computer modelling has become an effective tool adopted for the appraisal of the service condition

46 of concrete structures exposed to saline environments. There are a large number of publications

47 on the topic. Typically, the proposed models can be classified into two types. Type 1 uses Fick's

48 second law, which adopts an apparent diffusion coefficient to take account of the various

49 influences [13,14]. Type 2 explicitly describes the coupled pore water convection and chloride

50 diffusion mechanisms using a water infiltration model together with Fick's law [15]. The

51 environmental and the material factors, which link to the two transport mechanisms, can be

52 specified in the modelling [16] (for example, the influence of cylic wetting and drying conditions

53 [17-19], the effect of the electrical double layer at the pore surfaces [20], the osmotic effect [21],

54 and the effect of double-porosity in concrete [22]).

55 The cyclic wetting-drying and the osmotic effect together have a combined effect on both the

56 chloride diffusion and the pore water infiltration in concrete. However, so far, understanding and

57 quantifying the two coupled mechanisms are still limited [13,23]. Considering the two mechanisms

58 together with other factors, such as the pore structure of concrete [24-26], are reported upon even

59 less. Thus far, more systemic studies, from experiments to mathematic characterization, are still

60 required to evaluate these coupled mechanisms accurately aiming to provide a reliable tool for the

61 assessment of concrete durability exposed to chloride attack. As an effort to contribute to this

62 purpose, this paper initially reports on an experiment regarding the vapour-water absorption

63 isotherm of Portland cement concrete of different chloride content and porosity. Thereafter, a novel

64 characteristics' model based on the fundamental physics of vapour-water absorption is proposed

65 and validated using the experimental data. Finally, as a demonstration of a practical application,

66 the model is implemented to simulate chloride ingress in concrete in a region exposed to tidal

67 splash.

68

69 ## 2. Experiment

70 ### 2.1 Mix Design and Concrete Specimens

71 Locally produced Portland limestone cement, CEM II/A-LL conforming to the British standard

72 BS EN 197-1: 2011, was used for the concrete mixes at 390 kg/m^3. Natural sand of the maximum

73 size of 4.75 mm and a relative density of 2.47 was used for the fine aggregate at 580 kg/m^3. The

74 coarse aggregate was limestone of 10 mm maximum size and 2.49 specific gravity and used at

75 1125 kg/m^3. The mix of concrete followed the British standard, BS 1881-125:2013.

76

77 Four different chloride contents were prepared by adding NaCl in the mix water, they were 0, 1.5,

78 3 and 4.5% of the cement mass, respectively. Three different water to cement ratios (w/c) of 0.4,

79 0.5 and 0.6 were used for all these NaCl mixes. All the cast concrete samples were cured for 28

80 days by submerging in the water of the same chloride content as that used for their mixes. This

81 fully saturated curing method aims for an even distribution of chloride in the concrete samples

82 and, therefore, makes the test results more reliable. For each NaCl mix and w/c, three specimens

83 were prepared for individual specific property measuring, and the final result took the average of

84 the triplicate measurements.

85

86 ### 2.2 Vapour-Water Sorption Isotherm

87 After 28 days, all the cured saturated samples were weighed in their surface dry states. Thereafter,

88 they were put in environmental chambers with three controlled relative humidity (RH) values,

89 which were 35%, 60% and 80%, respectively. These samples were kept in the chambers at a

90 controlled temperature of 21°C for enough time until no weight change was observed (less than

91 0.001g). Then the equilibrium water content for each of the RH controlled conditions was

92 measured using the weighing method on an electrical scale of an accuracy of 0.001g. The results

93 presented the vapour-water sorption isotherm or the vapour absorption and water retention

94 characteristics of the concrete samples. Fig. 1 compares the measured equilibrium of (a) the pore

95 water content, and (b) the calculated corresponding pore water saturation (the ratio of unsaturated

96 pore water content to the fully saturated water content) in these concrete samples when exposed to

97 different environmental humidities. Table 1 presents the measured porosity of the concrete samples

98 using different w/c ratios. It can be seen that for the hardened concrete of a specific porosity, when

99 exposed to a certain environmental humidity, the higher the chloride salt content, the higher the

100 pore water content and the pore water saturation degree. The trend is particularly highlighted in

101 the lower middle range of the pore water saturation of 0.2~0.5 as shown in Fig. 1(b). This

102 phenomena can be explained by the enhanced capillary condensation in this range under high salt

103 content in both pore water and the solid matrix of concrete.

104

105   Table 1. Measured average concrete porosity vs w/c

w/c	0.4	0.5	0.6
Porosity	0.16	0.19	0.21

106
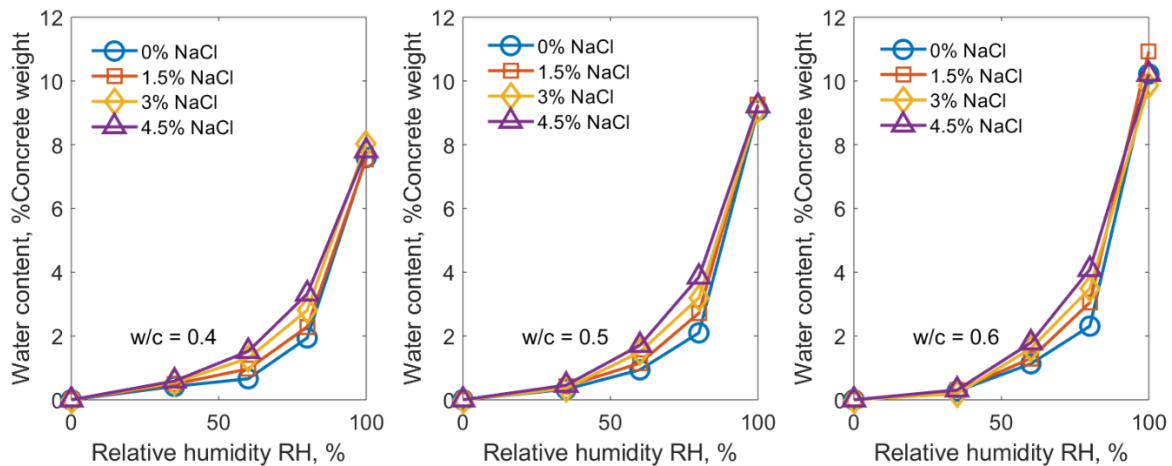
108   (a) Water content vs RH
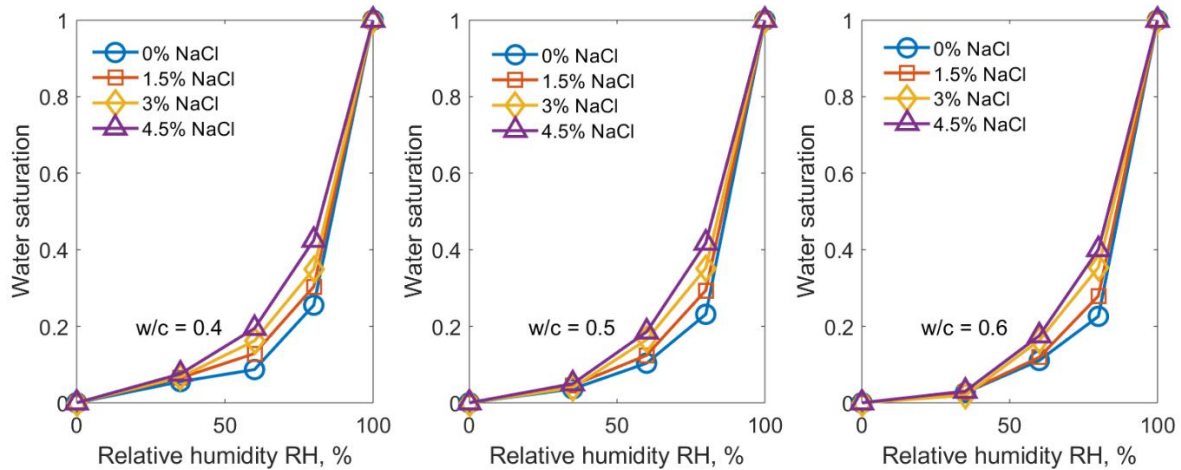
(b) Pore water saturation vs RH

Figure 1. Concrete water retention characteristics under different NaCl contents

Fig. 2 replots the data in Fig. 1 to compare the effect of porosity under the condition of the same chloride salt contents. It can be seen that the influence of the porosity on the vapour absorption and water retention characteristics is much less than that of the salt content. The porosity effect is particularly obvious at a low water saturation degree less than 0.2. In the range, it can be seen that, under the same environmental humidity, the lower the porosity the higher the water saturation, and the trend is further enhanced by a high NaCl content. This can be explained by the fact that the lower the porosity the higher the percentage of small pores. A large number of small pores increases both the total pore surface area and the water capillary condensation inside them.

1
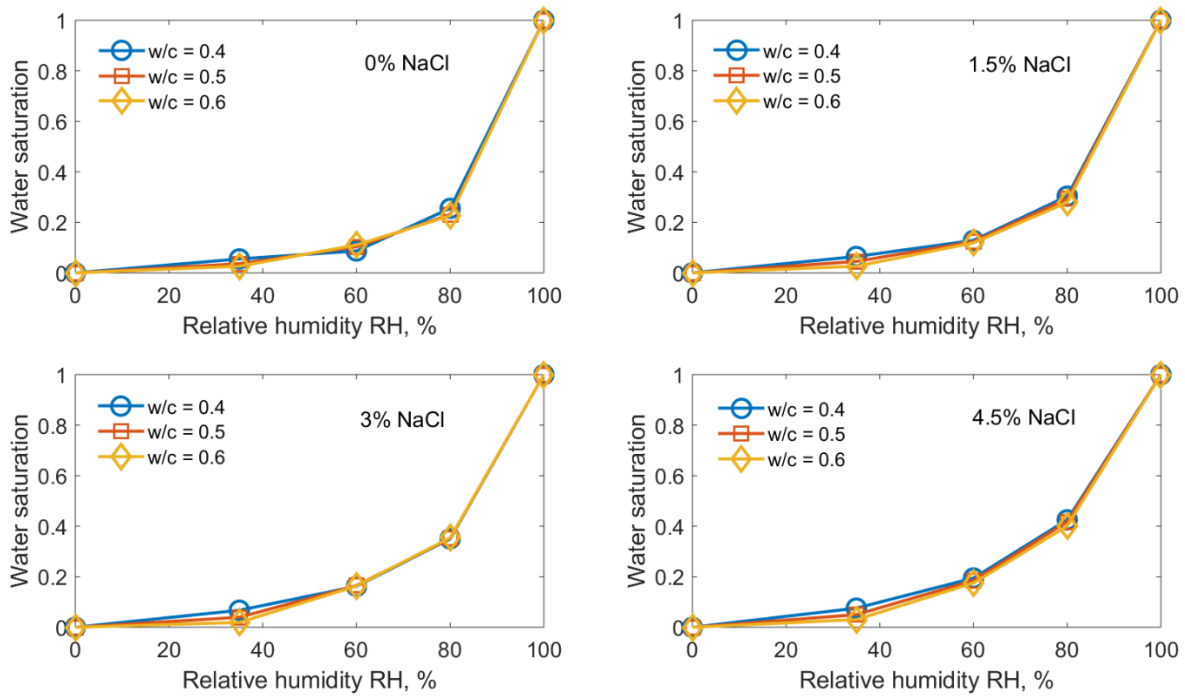
123   Figure 2. The effect of porosity on water retention characteristics

124

2.3 Chloride Binding Isotherm

126   At the end, all the samples of added NaCl were measured for their actual total and free chloride

127   contents after the submerged curing, respectively. Three cylindrical cores of the size 12 mm × 100

128   mm (diameter × length) evenly distributed along the central line of a cubic sample (100 mm × 100

129   mm × 100 mm) were taken from each mix sample and crushed into powder. The powder of the

130   three cylindrical cores were mixed together to represent the sample of each mixture. The test

131   followed the method specified in the standards [27,28]. Fig. 3 shows the measured free and total

132   chloride contents in terms of dry concrete weights of samples (using concrete weight rather than

133   cement weight is considered to be more convenient for in-situ practice). Four extra data in the

134   cases of w/c = 0.4 & 0.5 were obtained from the other samples prepared in another study [29]. It

135   can be seen that the measured free and total chlorides in the range of chloride contents present a

136   reasonable linear relationship. These fitting results show that the higher the w/c the higher the

137   slope of the fitting linear trend. It means that the bound chloride content in the concrete of higher

138   porosity decreases.

139
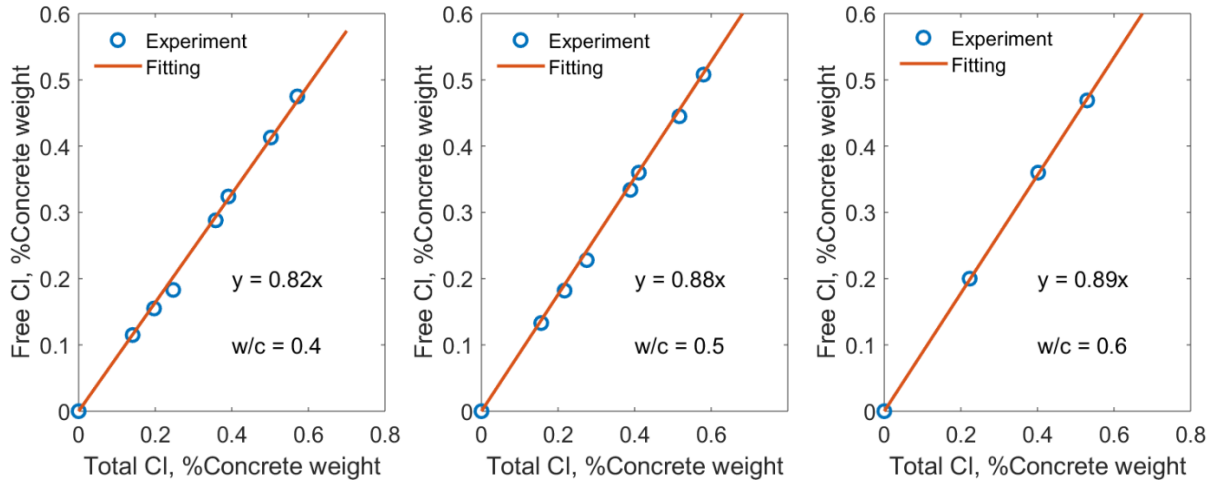
Figure 3. The relationship between the free and total chloride content

3. Vapour-Water Sorption Characterisation

The vapour-water sorption isotherm (VWSI) is an important property of concrete which plays an essential role in the modelling and analysis of moisture transport in concrete [30], and in the information for pore size distribution [31-33]. Although salty ions in concrete have a proven influence on the VWSI of concrete, so far, specific research on the topic is still limited. Particularly, more profound work is still necessary in order to provide a reliable mathematical characterisation model to quantify the influence. A previous research has suggested that the water retention in unsaturated porous materials is driven by the vapour absorption of the pore surface and the water condensation in pore voids due to the physical-chemical interfacial forces at pore surfaces [34]. This fundamental understanding generates an analytic mathematical model for the VWSI of hardened concrete as shown below [35,36]:

$$S_c = \lambda \left[\frac{1}{\beta} - \frac{1}{\alpha} + \frac{1}{\alpha} e^{\alpha S_w} - \frac{1}{\beta} e^{\beta(1-S_w)} \right] \qquad (1),$$

where S_c is capillary suction of unsaturated concrete, S_w is the pore water saturation in concrete, and α, β and λ are three interfacial physical-chemical parameters decided by material nature, pore structure and the interfacial forces at pore surfaces [34-36]. For engineering convenience purposes, it is suggested that Eq. (1) be simplified into the form of Eq. (2) below, where $f_0 = \lambda(\frac{1}{\beta} - \frac{1}{\alpha})$ and

161   the single parameter P_0 is adopted to reflect the coupled effect of the $\frac{\lambda}{\alpha}$, a term related to the water

162   phase in filled pores and $\frac{\lambda}{\beta}$, a term related to the vapour phase in co-existing empty pores [35].

163

164    $$S_c = f_0 + P_0\left[e^{\alpha S_w} - e^{\beta(1-S_w)}\right]$$ (2).

165

166   The simplified form of Eq. (2) has been not only successfully used for concrete VWSI modelling

167   [35] but has also been applied to other physical properties of other porous materials, such as soils

168   [36-38]. This paper revises Eq. (2) using an exponential weighing function to reflect the osmotic

169   effect of chloride on the water suction capacity of concrete. The proposed model takes the form of

170   Eq. (3) below:

171

172    $$S_c = e^{\gamma Cl}\left[f_0 + P_0\left(e^{\alpha S_w} - e^{\beta(1-S_w)}\right)\right]$$ (3),

173

174   where Cl is the chloride content, and γ is a constant parameter determined by fitting Eq. (3) to

175   experimental measurement.

176

177   To use Eqs. (2) and (3) to characterise the experimental data in Fig. 1, we need to work out the

178   concrete suction at different water contents. Under equilibrium with environmental moisture,

179   concrete suction can be evaluated in terms of the moisture relative humidity [39], i.e.:

180

181    $$S_c = |RTln(RH)/V_w|$$ (4),

182

183   where R is gas constant, T is the temperature in Kelvin, RH is relative humidity and V_w is the molar

184   volume of water.

185

186   Fig. 4 is a replot of the data in Fig. 1(b) by replacing the RH using S_c in terms of Eq. (4), assuming

187   a temperature of 21°C, and $V_w = 18.03 \times 10^{-6}$ m^3/mole. The modelling curves are the results of using

188   Eq. (2) to fit the experimental data. The fitting was conducted using MATLAB. The modelling

189   results show that Eq. (2) well represents the vapour absorption and the water retention

190   characteristics, i.e. the VWSI of concrete under certain chloride salt contents and porosity

191   conditions. The fitting curves in the cases of w/c = 0.5 and 0.6 do not reach the experimental data

192   of the full saturation condition S_w = 1. This may be explained as being due to microcracks in the

193   concrete samples, where pore water subjects a very small suction [33]. The fitting tool is beyond

194   its lowest accuracy at such low suction values. A further research is ongoing to address this issue.

195
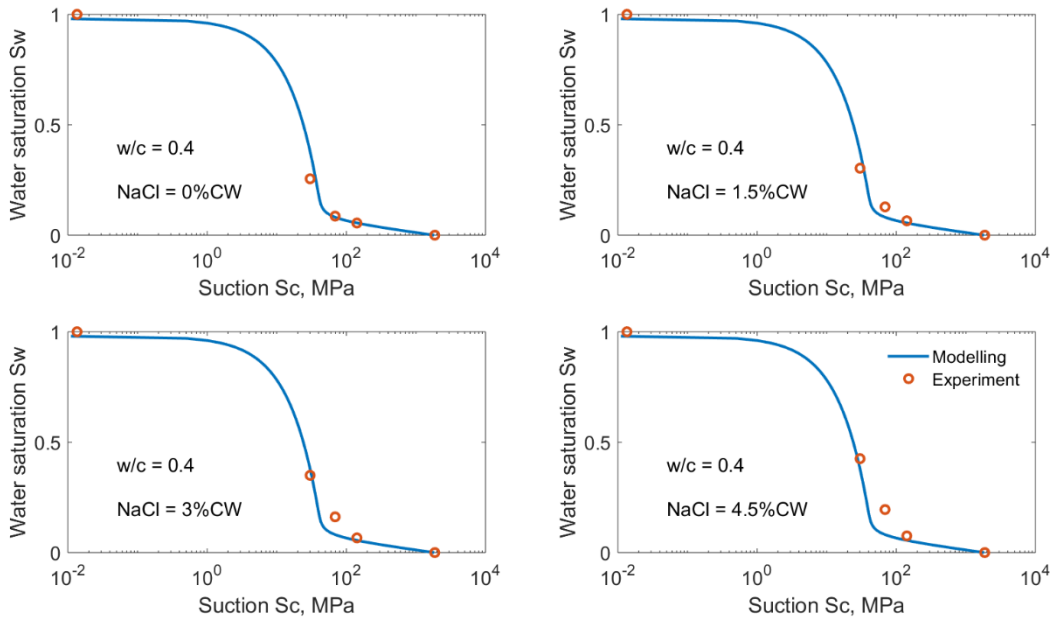
196

197   (a) w/c = 0.4
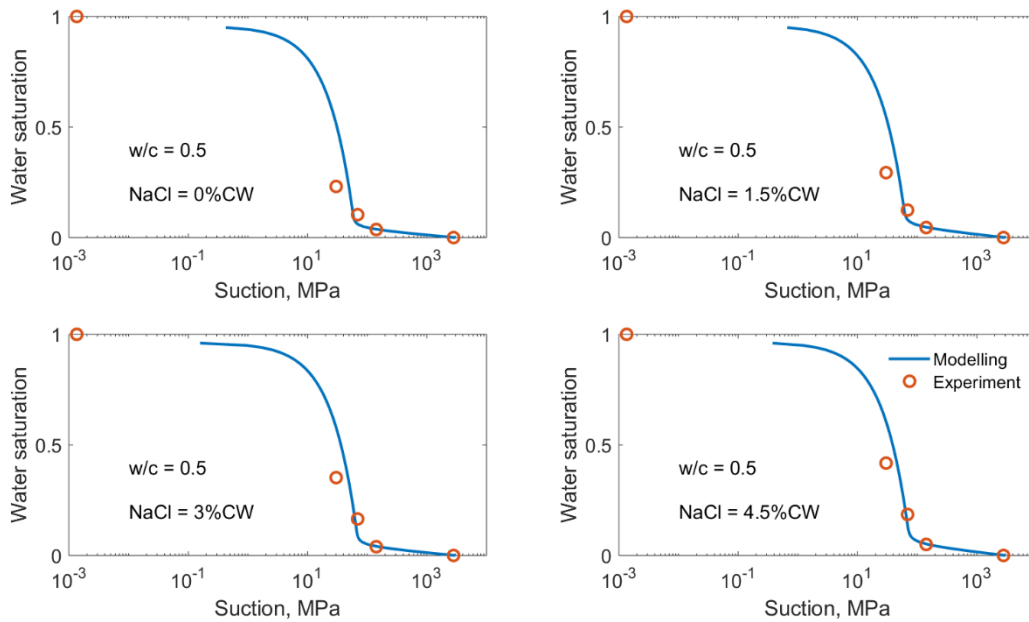
198

199   (b) w/c = 0.5

200
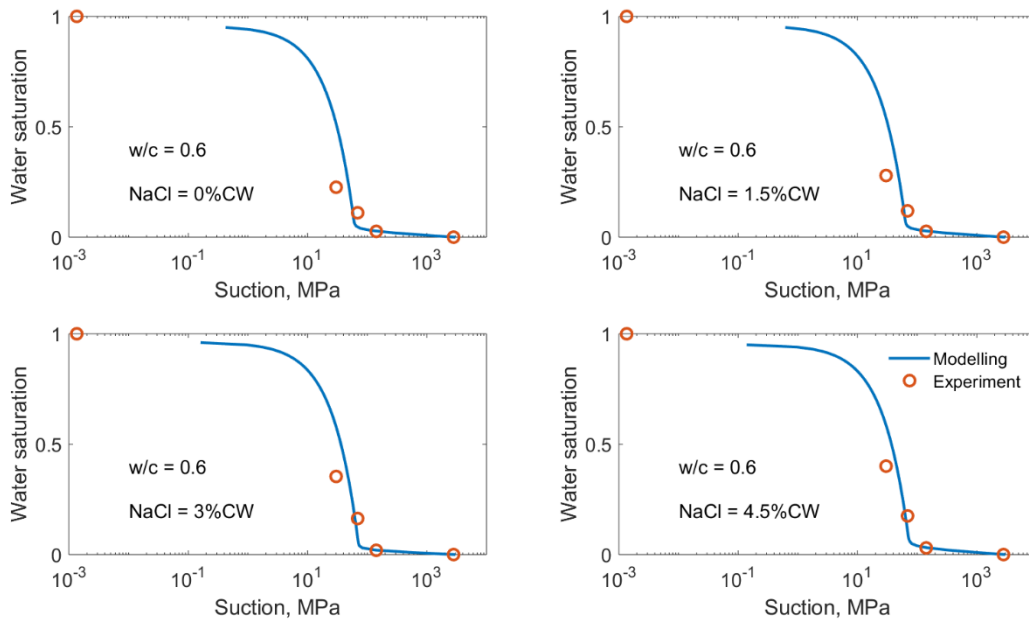
201   (c) w/c = 0.6

202   Figure 4. The modelled VWSI curves at certain chloride contents

203

204   Fig. 5 shows the results using Eq. (3) to fit all the experimental data in each specific w/c cases in

205   Fig. 4. All the data in each w/c case stands for a surface in the space of suction (S_c), pore water

206 saturation (S_w) and chloride content, where Cl/CW is the chloride content (Cl) in terms of the dry
207 concrete weight (CW) under a certain NaCl addition. The obtained characterisation surface
208 obtained using Eq. (3) to fit these experimental data well represents the VWIS in the whole range
209 of both the water and chloride contents except at a fully dry state. The fully dry state was excluded
210 when undertaking the surface fitting because it is hard to identify the starting point at a fully dry
211 state. Table 2 lists the corresponsive fitting parameter data obtained. The RMSE (root-mean-square
212 error) and the R-squared are defined as:

213

214 $$RMSE = \sqrt{\frac{\sum_{i=1}^{n}(y_i - f_i)^2}{n}} \tag{5},$$

215 $$R - squared = \sqrt{1 - \frac{\sum_{i=1}^{n}(y_i - f_i)^2}{\sum_{i=1}^{n}(y_i - \bar{y}_i)^2}} \tag{6},$$

216

217 where $\bar{y}_i$ is the average of all the experimental data y_i, n is the total number of the experimental
218 data, f_i is the modelling value from the data fitting. The lower the RMSE value the better the
219 modelling. Meanwhile, a value of R-squared closer to 1 indicates that the model has almost all the
220 variability of the response data around its mean.

221

222 Table 2. The obtained fitting parameters in Eq. (3) for the results in Fig. 4

w/c	γ	f_0	P_0	α	β	RMSE	R-square
0.4	0.9104	390.9	391.9	-25.76	-1.23	8.789	0.9811
0.5	0.3661	163.4	163.5	-11.96	-0.2762	7.777	0.9871
0.6	0.1867	137.9	137.8	-9.438	-0.2945	8.022	0.9862

223
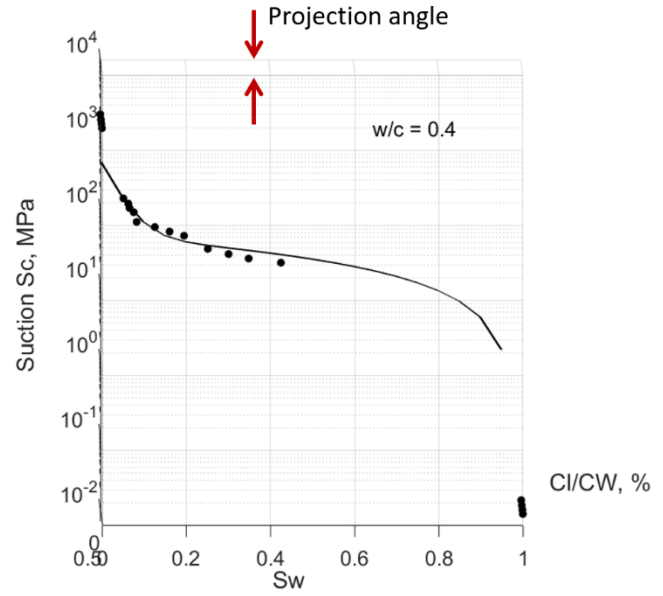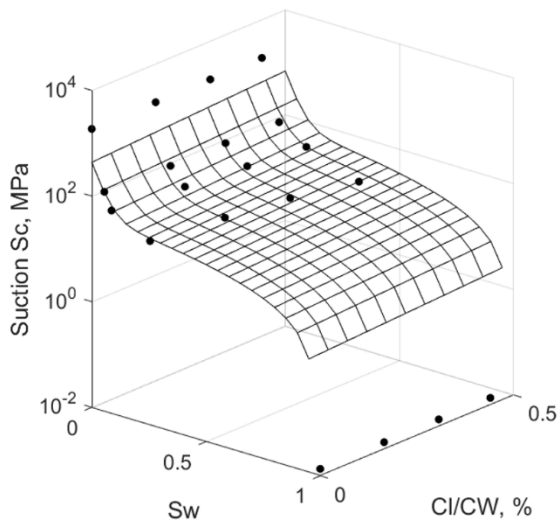
224

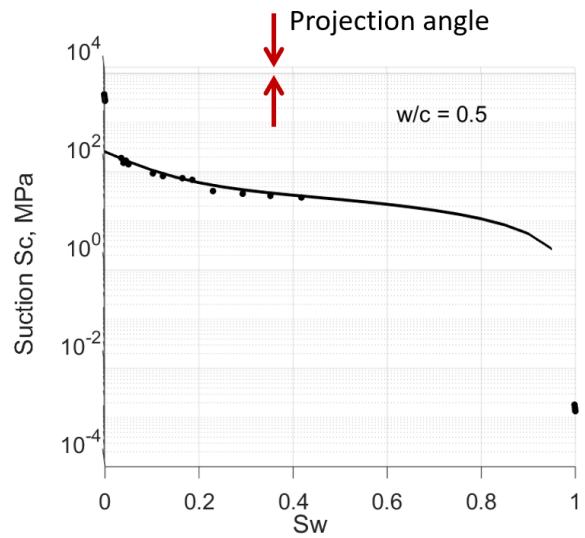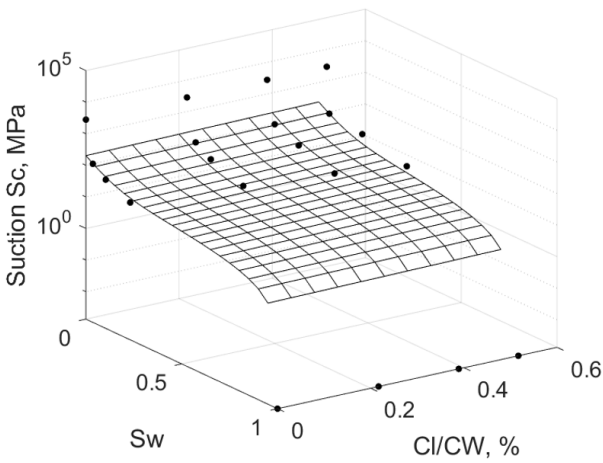225   Modelled VWSI surface   The projection on S_c-S_w plane

226   (a) w/c = 0.4
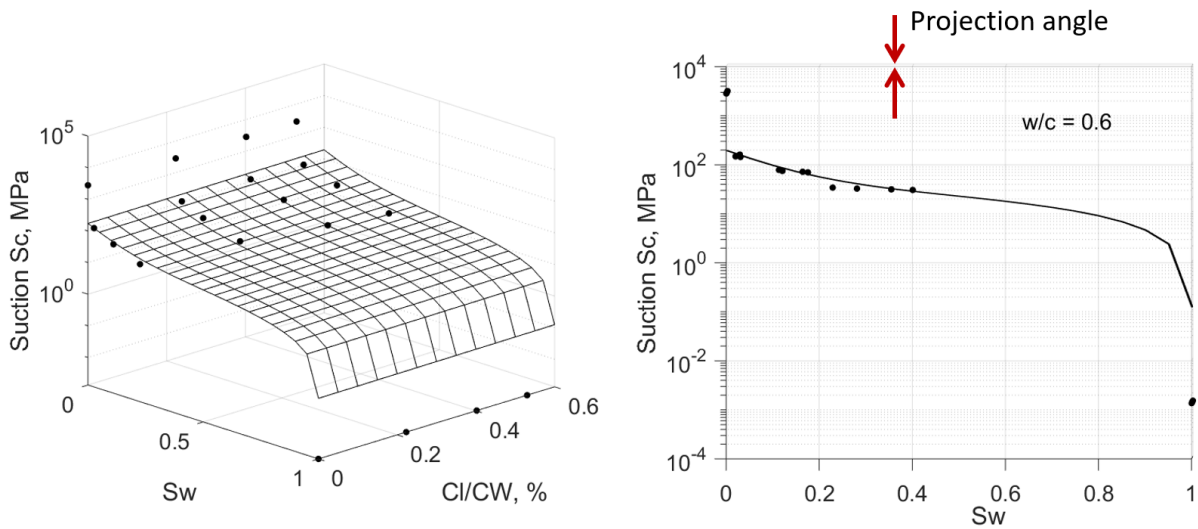
227

228

229   Modelled VWSI surface   The projection on S_c-S_w plane

230

231   (b) w/c = 0.5

232

Modelled VWSI surface   The projection on S_c-S_w plane

(c) w/c = 0.6

Figure 5. VWSI in 3D S_c-S_w-Cl/CW space

The projection angle, which reflects the effect of Cl, is to make the projection of the VWSI surface on the S_c-S_w plane (or in the axis of Cl/CW) close to a single curve. It can be seen that the higher the w/c the lower the projection angle, thus demonstrating the fact that the osmotic effect of the salt content on VWSI becomes less when concrete porosity increases.

4. Modelling Chloride Ingress in Tidal Zones

4.1. Modelling chloride transportation in unsaturated concrete

This paper incorporates Eq. (3) into a process model for chloride ingress in concrete. In terms of the ionic concentration in pore water, the governing equations for the ions' transport in concrete pore solution can be expressed as [3,40]:

$$\tau \frac{\partial}{\partial t}(C_i + S_i) = z_i \nabla \left[D_i \left(\frac{F}{RT} \nabla \phi \right) C_i \right] + \nabla(D_i \nabla(C_i)) - \tau \nabla(C_i v) \tag{7},$$

$$\frac{F}{RT} \nabla \phi = -\frac{\frac{\tau I}{F\varepsilon} + \sum_i^n z_i D_i \nabla C_i}{\sum_i^n z_i^2 D_i C_i} \tag{8}.$$

252   The left-hand-side of Eq. (7) stands for the rate of the local chloride concentration change, where

253   τ is the tortuosity of the pore network, C_i is the concentration of ionic species i, in concrete pore

254   water, t is time, S_i is the concentration of ionic species in concrete solid phase in terms of the pore

255   water volume. On the right-hand-side of Eq. (7), the first term stands for the ions' migration due

256   to the local electrical interaction between the ions (Eq. (8)), where z_i is the ions' charge number,

257   F is the Faraday's constant, R is gas constant, T is kelvin temperature, D_i is the diffusion

258   coefficient of ions in pore water, ϕ is the local electrostatic potential in pore water, n is the total

259   number of ionic species in concrete pore water, I is the electrical current density applied externally

260   on the concrete, such as in case of cathodic protection. For the following case study in the next

261   section 4.2, there is no external applied electrical current, i.e. $I = 0$. The second term stands for the

262   ions' diffusion under concentration gradient. The third term stands for the ions' convection with

263   the flow of pore water, where v is the superficial velocity of bulk pore water in concrete.

264

265   For unsaturated concrete, to close Eqs. (7) and (8), the pore water velocity, v, is required. Water

266   flow in porous media is a topic of hydrology. The water flow in pores is driven by two forces, i.e.,

267   the gravity due to elevation and the capillary suction at an unsaturated state. The flow driven by

268   the latter is called wick action. The first one is proportional to the gradient of the water head, while

269   the second one is fundamentally linked to the pore water saturation degree and the VWSI. An

270   unsaturated flow theory [41] was developed by extending the original Darcy's law for a saturated

271   state to an unsaturated state. The modified Darcy equation takes the form below:

272

273    $$v = -K_w \nabla(p + \rho g z) \tag{9},$$

274

275   where v is the superficial velocity of pore water, K_w is hydraulic conductivity, p is the capillary

276   suction in negative value, and $\rho g z$ is the gravity potential given water density ρ, gravity g and

277   elevation z. Both K_w and p depend on the water saturation degree. If we neglects the elevation

278   effect, by substituting a negative value of S_c of Eq. (3) into Eq (9) for p, we obtain:

279

280    $$v = -K_w \nabla(-S_c) = -K_w \frac{\partial(-S_c)}{\partial S_w} \nabla S_w \tag{10}.$$

281

282   Rewriting Eq. (10) into the form below:

283

284 $$v = -D_w \nabla S_w \tag{11},$$

285

286   where $D_w = K_w \frac{\partial(-S_c)}{\partial S_w} = K_w e^{aCl}\left[-P_0\left(\alpha e^{\alpha S_w} + \beta e^{\beta(1-S_w)}\right)\right]$ is called hydraulic diffusivity. In

287   addition, water flow in concrete also meets the mass conservation, i.e.:

288

289 $$\frac{dS_w}{dt} = -\nabla v \tag{12}.$$

290

291   Substituting Eq. (11) into Eq. (12), we at last have:

292

293 $$\frac{dS_w}{dt} = \nabla(D_w \nabla S_w) \tag{13}.$$

294

295   Now Eqs. (7), (8), (11) and (13) are closed. They deterministically define ions' transport in

296   unsaturated concrete. In the next section, we applied the closed equation system to simulate a

297   concrete column exposed in a tidal zone.

298

299   **4.2. A simulation case study**

300   A 2m high concrete (w/c = 0.4) column with a diameter of 1m stands in salty water of 1m depth.

301   It is assumed that 0.5 meter above the bulk water surface level is subject to tidal splash. Assuming

302   that the average environmental humidity is RH = 75%, and referring to the data in Fig. 2, the initial

303   and boundary conditions are defined as:

304   1. $S_w = 1$, h <= 1 m (h is the vertical height along the column),

305   2. $S_w = 0.2$, h > 1.5 m,

306   3. At the concrete surface in a tidal zone (h = 1 ~ 1.5 m), $S_w = \max(\sin(\pi/12 \times t), 0.2)$ (t is time

307   in hours), as showed in Fig. 6.

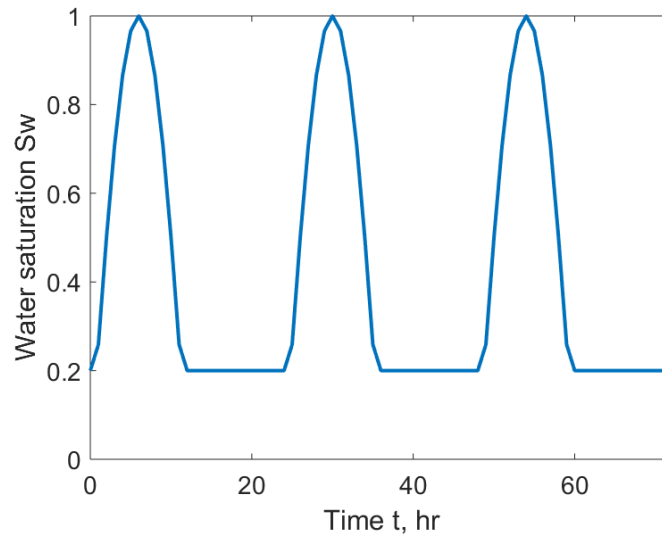308   A hydraulic conductivity model for unsaturated flow in hydrology is adopted [39], which is:

309

310 $$K_w = K_s S_w^{\,n} \tag{14},$$

311

312   where K_s is saturated hydraulic conductivity.

313

314
315   Figure 6. Boundary condition in the tidal zone

316

317   Salty water is assumed to be a solution of 479 mole/m^3 NaCl. Four main types of ions in concrete

318   pore water are taken into account by hypothesis; they are chloride (Cl$^-$), sodium (Na$^+$), potassium

319   (K$^+$) and hydroxide (OH-). The other parameters and initial data adopted are listed in Table 3 (the

320   data in Table 3 are based purely on assumption and refer to some information presented in previous

321   publications [3,40]. However, there is some most recent work [42,43] that can be referred to, which

322   will help the selected data to be closer to reality).

323

324   Table 3. Parameters and data used in simulation

Eqs. (7) & (8)				
	Cl$^-$	Na$^+$	K$^+$	OH$^-$
Diffusion coefficient, D_i m^2/s	2.03×10^{-9}	1.334×10^{-9}	1.957×10^{-9}	5.27×10^{-9}
Initial concentration in concrete mole/m^3	5	5	490	[OH$^-$] + [Cl$^-$] = [Na$^+$] + [K$^+$]
Tortuosity, τ	2			
Porosity, ε	0.167			

| Bound Chloride	$S_{cl} = 0.223\ C_{Cl}$
Mole/m^3	In terms of the linear relationship in Fig. 2
Eq. (14)	
K_s	$5×10^{-16}$
(m/s)	
n	2

325

326

4.3. Modelling results

Fig. 7 shows the water saturation degree and the chloride profile in the symmetric half of the column at the initial stage and after exposure to tidal splash for one year. It can be seen that cyclic tidal splash accelerates the chloride ingress into the concrete at the region of the bulk water surface $(y = 1m)$. Fig. 8 compares the chloride profiles in the column at the bottom underwater $(y = 0)$ and at the level of the bulk water surface $(y = 1m)$ after 1 year. It can be seen that both splash and osmotic effects have enhanced the chloride ingress in the tidal region, but water splash is much more significant than the osmotic action in terms of influence.
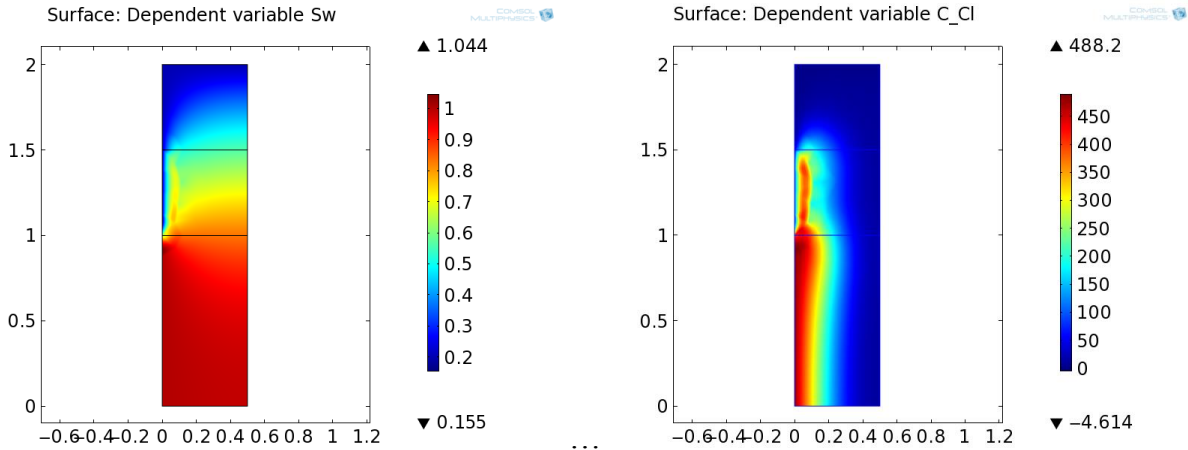
335
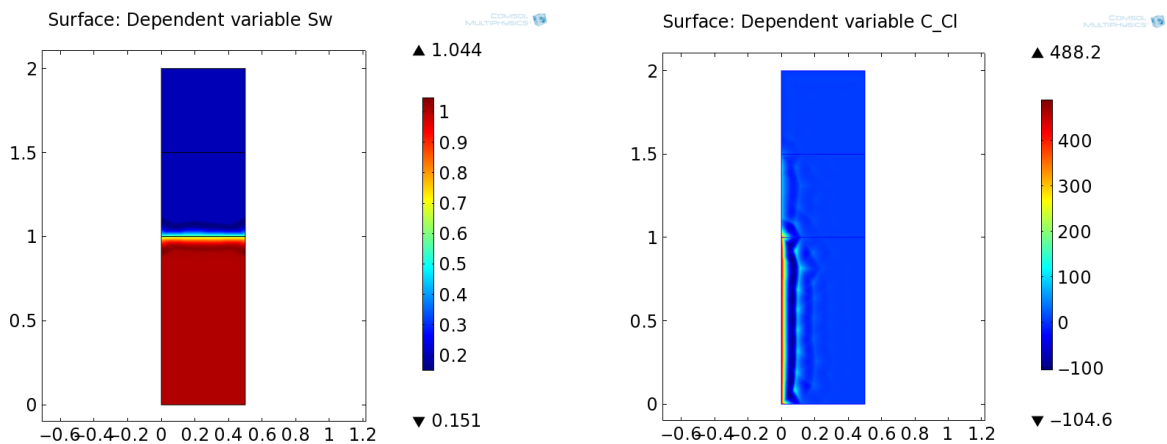
(a) Water saturation (b) Chloride concentration, mole/m^3

(a). Initial condition, t = 0 hr

339
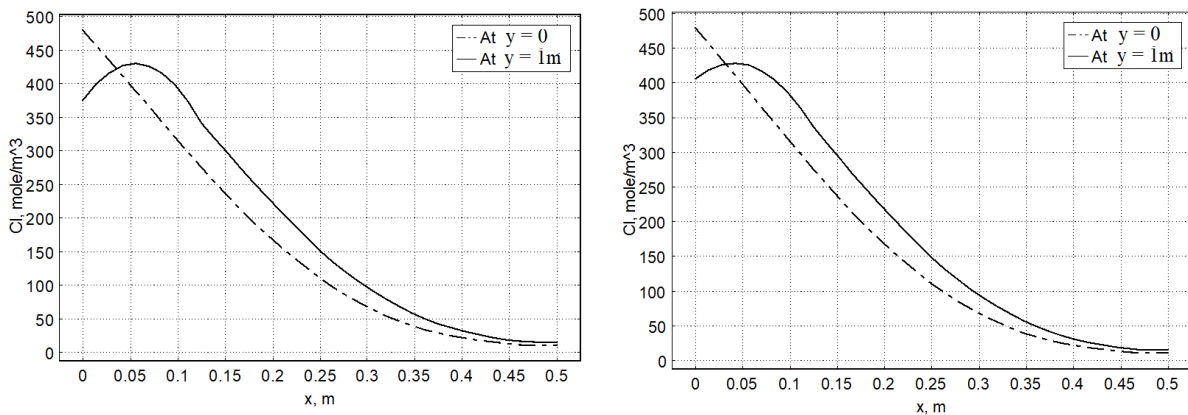
(a) Water saturation (b) Chloride concentration, mole/m^3

(b). After 1 year, t = 8736 hr

Figure 7. Water saturation and the chloride profile in the concrete column

(a) With osmotic effect (b) Without osmotic effect ($\gamma = 0$ in Eq. (3))

Figure 8. Comparison of the chloride profile

Fig. 9 shows the water saturation degree in concrete at the height of the external bulk water surface level after 1 year's exposure. It shows that osmotic action has enhanced the water ingress as the local water saturation in concrete has increased with different degrees, while the highest increase is at the depth of x = 0.1 m.

354

...
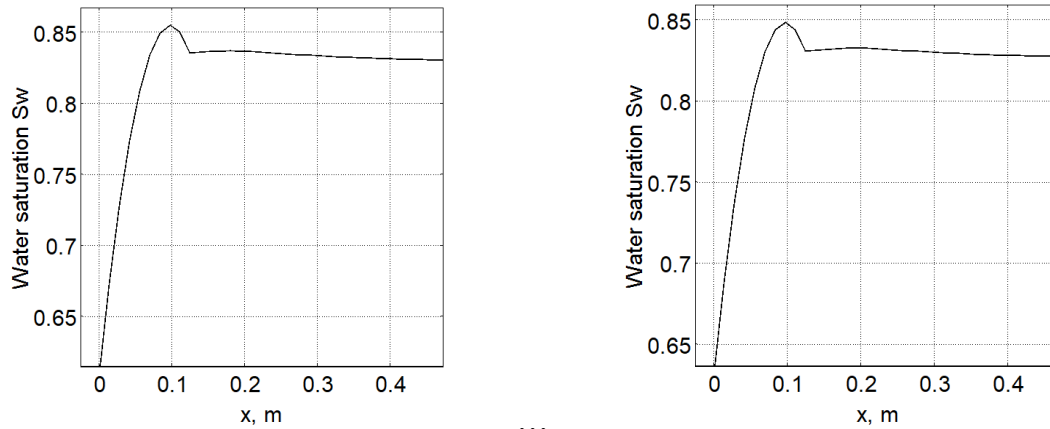
(a) With osmotic effect   (b) Without osmotic effect ($\gamma = 0$ in Eq. (3))

Figure 9. The water saturation degree in concrete at the height y = 1m

5. Conclusions

This paper presents an experimental study of the chloride salt effect on the vapour-water sorption isotherm of concrete. An effective characteristic model has been proposed and validated using experimental data. The model has been successfully implemented to simulate chloride ingress in concrete structures in tidal zones. The following conclusions can be drawn:

1. Chloride salt in concrete will increase the concrete water content or the pore water saturation degree when exposed to the same environmental humidity due to osmotic action.
2. The osmotic effect on the vapour-water sorption isotherm can be effectively characterised using a proposed mathematical model.
3. Chloride ingress in concrete is significantly increased in the underwater region in a tidal zone.
4. Osmotic action has an influence on chloride diffusion in concrete but has a much lesser influence on water ingress.

378

6. References

[1] G. Sergi, S. Yu, C. Page, Diffusion of chloride and hydroxyl ions in cementitious materials exposed to a saline, Magazine of Concrete Research 44(158) (1992) 63-69.

[2] K. Maekawa, T. Ishida, Modeling of structural performances under coupled environmental and weather actions, Materials and Structures 35(10) (2002) 591-602.

[3] Y. Wang, L.-Y. Li, C. Page, Modelling of chloride ingress into concrete from a saline environment, Building and Environment 40(12) (2005) 1573-1582.

[4] G. Lin, Y. Liu, Z. Xiang, Numerical modeling for predicting service life of reinforced concrete structures exposed to chloride environments, Cement and Concrete Composites 32(8) (2010) 571-579.

[5] P. Zhang, D. Hou, Q. Liu, Z. Liu, J. Yu, Water and chloride ions migration in porous cementitious materials: An experimental and molecular dynamics investigation, Cement and Concrete Research 102 (2017) 161-174.

[6] A. Ababneh, F. Benboudjema, Y. Xi, Chloride penetration in nonsaturated concrete, Journal of Materials in Civil Engineering 15(2) (2003) 183-191.

[7] D. Conciatori, H. Sadouki, E. Brühwiler, Capillary suction and diffusion model for chloride ingress into concrete, Cement and Concrete Research 38(12) (2008) 1401-1408.

[8] S. Meijers, J. Bijen, R. De Borst, A. Fraaij, Computational results of a model for chloride ingress in concrete including convection, drying-wetting cycles and carbonation, Materials and Structures 38(2) (2005) 145-154.

[9] E. Samson, J. Marchand, K.A. Snyder, J. Beaudoin, Modeling ion and fluid transport in unsaturated cement systems in isothermal conditions, Cement and Concrete Research 35(1) (2005) 141-153.

[10] K. Hong, R. Hooton, Effects of cyclic chloride exposure on penetration of concrete cover, Cement and Concrete Research 29(9) (1999) 1379-1386.

[11] Z. Yu, Y. Chen, P. Liu, W. Wang, Accelerated simulation of chloride ingress into concrete under drying–wetting alternation condition chloride environment, Construction and Building Materials 93 (2015) 205-213.

[12] J. Wu, H. Li, Z. Wang, J. Liu, Transport model of chloride ions in concrete under loads and drying-wetting cycles, Construction and Building Materials 112 (2016) 733-738.

409 [13] Y. Zhang and W.-L. Jin, Distribution of Chloride Accumulation in Marine Tidal Zone along

410 Altitude, ACI Materials Journal (2011) 1-9.

411 [14] R.A. de Medeiros-Junior, M.G. de Lima, P.C. de Brito, M.H.F. de Medeiros, Chloride

412 penetration into concrete in an offshore platform-analysis of exposure conditions, Ocean

413 Engineering 103 (2015) 78-87.

414 [15] C. Sun, L. Yuan, X. Zhai, F. Qu, Y. Li, B. Hou, Numerical and experimental study of

415 moisture and chloride transport in unsaturated concrete, Construction and Building Materials 189

416 (2018) 1067-1075.

417 [16] B.H. Oh, S.Y. Jang, Effects of material and environmental parameters on chloride

418 penetration profiles in concrete structures, Cement and Concrete Research 37(1) (2007) 47-53.

419 [17] A. Van der Zanden, A. Taher, T. Arends, Modelling of water and chloride transport in

420 concrete during yearly wetting/drying cycles, Construction and Building Materials 81 (2015)

421 120-129.

422 [18] Q.-Z. Zhang, X.-L. Gu, Z.-L. Jiang, W.-P. Zhang, Similarities in Accelerated Chloride Ion

423 Transport Tests for Concrete in Tidal Zones, ACI Materials Journal 115(4) (2018) 499-507.

424 [19] A. Petcherdchoo, Closed-form solutions for modeling chloride transport in unsaturated

425 concrete under wet-dry cycles of chloride attack, Construction and Building Materials 176

426 (2018) 638-651.

427 [20] P. Nguyen, O. Amiri, Study of electrical double layer effect on chloride transport in

428 unsaturated concrete, Construction and Building Materials 50 (2014) 492-498.

429 [21] J. Geng, L.-Y. Li, Y. Wang, Modelling of chloride penetration in unsaturated concrete,

430 Advances in Cement Research 28(1) (2015) 51-61.

431 [22] D. Li, L.-Y. Li, X. Wang, F. Xing, A double-porosity model for water flow in unsaturated

432 concrete, Applied Mathematical Modelling 53 (2018) 510-522.

433 [23] A.B. Fraj, S. Bonnet, A. Khelidj, New approach for coupled chloride/moisture transport in

434 non-saturated concrete with and without slag, Construction and Building Materials 35 (2012)

435 761–771.

436 [24] C. Zhou, Prediction water permeability and relative gas permeability of unsaturated cement-

437 based material from hydraulic diffusivity, Cement and Concrete Research 58 (2014) 143-151.

438 [25] S. Saliba, P. Ruch, W. Volksen, T.P. Magbitang, G. Dubois, B. Michel, Microporous and

439 Mesoporous Materials 226 (2016) 221-228.

440 [26] Q. Zeng, D.D. Zhang, H. Sun, K. Li, Characterizing pore structure of cement blend pastes

441 using water vapour sorption analysis, Materials Characterisation 95 (2014) 72-84.

442 [27] ASTM C1152/C1152M, Standard test method for acid-soluble chloride in mortar and

443 concrete, in, ASTM International, West Conshohocken, PA, USA, 2012.

444 [28] ASTM C1218/C1218M, Standard test method for water-soluble chloride in mortar and

445 concrete, in, ASTM International, West Conshohocken, PA, USA, 2015.

446 [29] H.M. Oleiwi, Y. Wang, M. Curioni, X-Y Chen, G-W Yao, Augusthus-Nelson L., Ragazzon-

447 Smith A.H., Shabalin I., An experimental study of cathodic protection for chloride contaminated

448 reinforced concrete, Materials and Structures 51 (2018) 148.

449 [30] V. Baroghel-Bouny, M. Mainguy, T. Lassabatere, O. Coussy, Characterization and

450 identification of equilibrium and transfer moisture properties for ordinary and high-performance

451 cementitious materials, Cement Concrete Research 29 (1999) 1225–38.

452 [31] C.G. Shull, The determination of pore size distribution from gas adsorption data, Journal of

453 the American Chemical Society, 70 (1948) 1405–10.

454 [32] V. Baroghel-Bouny, Water vapour sorption experiments on hardened cementitious materials:

455 Part I: essential tool for analysis of hygral behaviour and its relation to pore structure, Cement

456 Concrete Research 37 (2007) 414–37.

457 [33] Z. Wu, H.S. Wong, C. Chen, N.R. Buenfeld, Anomalous water absorption in cement-based

458 materials caused by drying shrinkage induced microcracks, Cement and Concrete Research; 115

459 (2019) 90-104.

460 [34] Y. Wang, S.M. Grove, M.G. Anderson, A physical-chemical model for the static water

461 retention characteristic of unsaturated porous media. Advances in Water Resources, 31 (2008)

462 723–735.

463 [35] Y. Wang, X. Wang, M. Scholz, D. Ross, A physico-chemical model for the water vapour

464 sorption isotherm of hardened cementitious materials, Construction and Building Materials 35

465 (2012) 941-946.

466 [36] Y. Wang, Phase deterministic modelling of water retention in unsaturated porous media and

467 its potential in dynamic unsaturated flow application, Journal of Porous Media 13 (2010) 261–

468 270.

469   [37] H. Jin, Y. Wang, Q. Zheng, H. Liu, E. Chadwick, Experimental Study and Modelling of the

470   Thermal Conductivity of Sandy Soils of Different Porosities and Water Contents, Applied

471   Science 7 (2017) 119.

472   [38] N. Xiang, Y. Wang, H.M. Oleiwi, E. Chadwick, G-W. Yao, L. Augusthus-Nelson, X-Y.

473   Chen, I. Shabalin, Modelling the electrical resistivity of concrete with varied water and chloride

474   contents, Magazine of Concrete Research (2019).

475   [39] D. Hillel, Environmental Soil Physics, 1st Edition, Adademic Press, 1998.

476   [40] Y. Wang, Chloride Transport in Concrete: Mathematical Description and Modelling. VDM

477   Verlag Dr. Müller 2011; Riga, Latvia.

478   [41] J.R. Philip, Theory of infiltration, Advance Hydroscience, 5 (1969) 215-296.

479   [42] M.H.N.Yio, H.S.Wong, N.R.Buenfeld, 3D pore structure and mass transport properties of

480   blended cementitious materials, Cement and Concrete Research 117 (2019) 23-37.

481   [43] M.H.N. Yio, M.J. Mac, H.S. Wong, N.R. Buenfeld, 3D imaging of cement-based materials at

482   submicron resolution by combining laser scanning confocal microscopy with serial sectioning,

483   Journal of Microscopy, 258 (2015)151-169.

484

485

486